Natural chromatin is heterogeneous and self-associates in vitro

Shujun Cai, Yajiao Song, Chen Chen, Jian Shi, and Lu Gan*
Department of Biological Sciences and Centre for BioImaging Sciences, National University of Singapore, Singapore 117543

ABSTRACT The 30-nm fiber is commonly formed by oligonucleosome arrays in vitro but rarely found inside cells. To determine how chromatin higher-order structure is controlled, we used electron cryotomography (cryo-ET) to study the undigested natural chromatin released from two single-celled organisms in which 30-nm fibers have not been observed in vivo: picoplankton and yeast. In the presence of divalent cations, most of the chromatin from both organisms is condensed into a large mass in vitro. Rare irregular 30-nm fibers, some of which include face-to-face nucleosome interactions, do form at the periphery of this mass. In the absence of divalent cations, picoplankton chromatin decondenses into open zigzags. By contrast, yeast chromatin mostly remains condensed, with very few open motifs. Yeast chromatin packing is largely unchanged in the absence of linker histone and mildly decondensed when histones are more acetylated. Natural chromatin is therefore generally nonpermissive of regular motifs, even at the level of oligonucleosomes.

Monitoring Editor
Susan Strome
University of California, Santa Cruz

Received: Jul 10, 2017
Revised: Apr 10, 2018
Accepted: May 4, 2018

INTRODUCTION

Eukaryotic chromatin structure is dictated by the three-dimensional relationship between nucleosomes (~146 base pairs of DNA wrapped around eight histones). Chromatin can adopt higher-order structures of varying condensation levels, which are influenced by factors like histone posttranslational modifications and interactions with chromatin "architectural" proteins (Jenuwein and Allis, 2001; McBryant *et al.*, 2006). Nucleosomes connected by linker DNA are traditionally described as "beads-on-a-string" (Olins and Olins, 1974). This beads-on-a-string chromatin is hypothesized to condense into a helical arrangement called the "30-nm fiber," which can be either a one-start solenoid or a two-start zigzag (Finch and Klug, 1976; Woodcock *et al.*, 1984). However, more than one form of nucleosome packing might also coexist in the same 30-nm fiber (Grigoryev *et al.*, 2009). The way in which nucleosome chains fold into these fibers is thought to control the accessibility of DNA to transcription and replication machines (Tse *et al.*, 1998; Collins *et al.*, 2002).

The diversity of observed chromatin structures has led to inconsistent terminology. For the sake of clarity, we define a chromatin "mass" as a dense, irregularly packed chromatin body; an "irregular 30-nm fiber" as a variable-width fiberlike structure with few repeated nucleosome motifs; a "regular 30-nm fiber" as an ordered compact structure ~30 nm wide; an "open zigzag" as a more-extended structure with exposed linker DNA and few nucleosome–nucleosome interactions; "beads-on-a-string" as a chain of nucleosomes in which the angle between the entering and exiting linker DNA is nearly 180°; and "10-nm filaments" as a linear chain of nucleosomes, all packed face to face (Figure 1A).

Most of our knowledge of chromatin structure comes from studies of dilute solutions of short nucleosomes chains. These studies have tested the effects of fixation with glutaraldehyde (Athey *et al.*, 1990), recombinant histones (Luger *et al.*, 1997b), linker histones (Routh *et al.*, 2008), artificially selected "Widom 601" sequences that have a high-affinity for histones (Dorigo *et al.*, 2004), and ionic conditions (Dorigo *et al.*, 2003; Huynh *et al.*, 2005). Under special conditions, such chromatin constructs can form highly regular 30-nm fibers that can be studied at high resolution (Song *et al.*, 2014). Furthermore, short nucleosome chains can oligomerize in the presence of magnesium ions without forming 30-nm fibers (Maeshima *et al.*, 2016).

This article was published online ahead of print in MBoC in Press (http://www.molbiolcell.org/cgi/doi/10.1091/mbc.E17-07-0449) on May 9, 2018.

Author contributions: S.C. performed experiments, project design, and writing; Y.S. performed experiments; C.C. performed experiments and editing; J.S. performed training; L.G. performed experiments, project design, and writing.

*Address correspondence to: Lu Gan (lu@anaphase.org).

Abbreviations used: cryo-EM, electron cryomicroscopy; cryo-ET, electron cryotomography; NND, nearest-neighbor distance; TSA, trichostatin A.

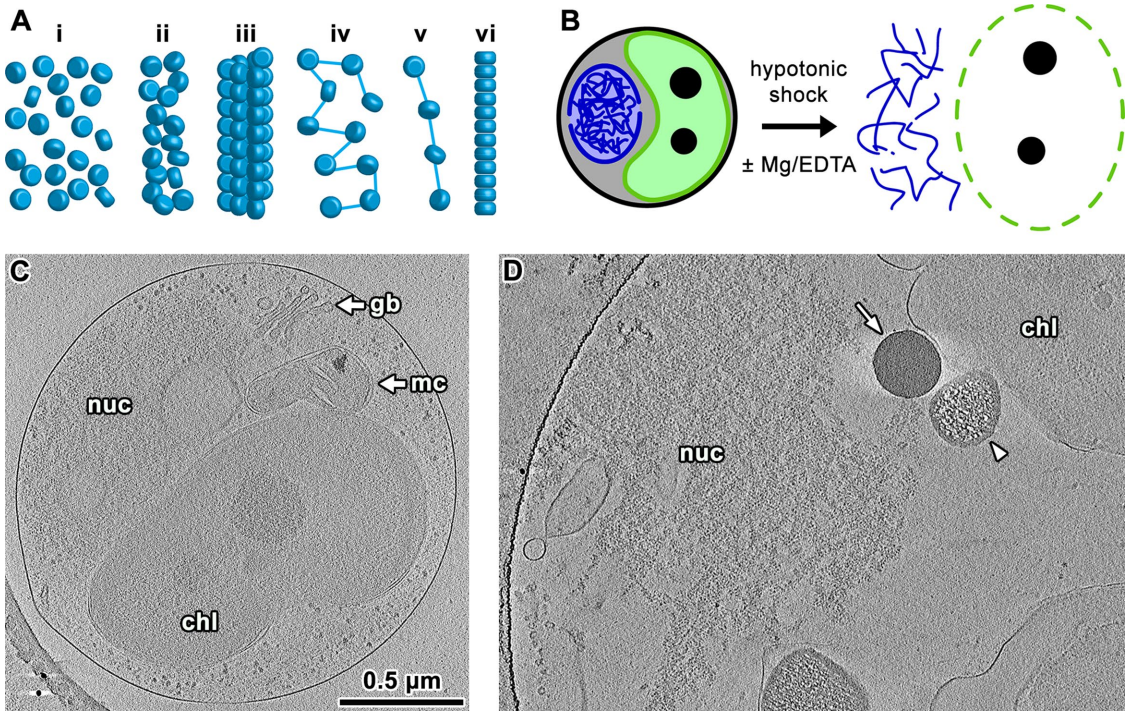

FIGURE 1: Strategy for three-dimensional analysis of natural chromatin. (A) Possible nucleosome arrangements, including (i) chromatin masses, (ii) irregular 30-nm fibers, (iii) regular 30-nm fibers, (iv) open zigzags, (v) beads on a string, and (vi) 10-nm filaments. Blue cylinders, nucleosomes; blue lines, linker DNA. (B) The plasma membrane (black line) is ruptured by hypotonic shock, exposing the cellular contents to buffer with or without Mg or EDTA added. The chloroplast (green) and nucleus (blue) are the two largest organelles in picoplankton. The nuclear and plasma membranes are completely disrupted, while the chloroplast membrane is partially disrupted (green circle). (C) Tomographic slice (30 nm) of an intact early-interphase picoplankton cell. The largest organelles are labeled: chloroplast (chl); nucleus (nuc); Golgi body (gb); mitochondrion (mc). The lower-left corner shows the curved edge of the carbon support and two gold fiducials (dark puncta). As previously observed, the nucleus does not have an intact nuclear envelope. (D) Tomographic slice (30 nm) of a lysed picoplankton cell in 1 mM Mg, at the same scale as in C. The arrow points to a radiation-tolerant granule, and the arrowhead points to a radiation-sensitive granule; both types of granules were originally inside the chloroplast. The nuclear (nuc) and chloroplast (chl) remnants are labeled. The lysed cell is flattened by surface tension (after blotting), causing all components to spread out.

Chromatin structure has also been studied in situ in a lifelike frozen-hydrated state, either in two dimensions by electron cryomicroscopy (cryo-EM) projection imaging or in three dimensions by electron cryotomography (cryo-ET). In situ studies are much rarer because it is challenging to thin the cells at cryogenic temperatures. In the late 1980s, a seminal cryo-EM study first challenged the notion that the in situ organization of mammalian chromatin is folded as regular 30-nm fibers (McDowall *et al.*, 1986). This conclusion was supported by follow-up cryo-EM studies (Eltsov *et al.*, 2008; Eltsov *et al.*, 2014). We have used cryo-ET to study chromatin in two single-celled organisms, *Ostreococcus tauri* (a eukaryotic picoplankton; herein called picoplankton) and *Saccharomyces cerevisiae* (a budding yeast; herein called yeast). In these organisms, there was also no evidence of regular 30-nm fibers (Gan *et al.*, 2013; Chen *et al.*, 2016). In contrast, cryo-EM and cryo-ET studies have respectively detected regular 30-nm fibers in the isolated nuclei of starfish sperm (Woodcock, 1994) and chicken erythrocytes (Scheffer *et al.*, 2011). Small-angle x-ray scattering studies have shown that chicken erythrocyte nuclei, but not human mitotic chromosomes, have 30-nm fibers (Nishino *et al.*, 2012). These and other studies suggest that 30-nm fibers may only be abundant in some classes of transcriptionally inactive cells (van Holde and Zlatanova, 1995; Hansen, 2012; Nishino *et al.*, 2012).

A recent study presented the "ChromEMT" approach to stain chromatin inside of cells (Ou *et al.*, 2017). Unlike cryo-ET, in which cells are both thinned and imaged in a frozen-hydrated state, ChromEMT requires cells to be fixed, dehydrated, heavy-metal stained, and plastic embedded. In the electron tomograms of these samples, there was no evidence of 30-nm fibers. The stain made irregular deposits that were 5 to 24 nm wide. These tomograms led to a conclusion that was consistent with earlier cryo-EM and traditional EM studies of mammalian cells (McDowall *et al.*, 1986; Eltsov *et al.*, 2008, 2014; Maeshima *et al.*, 2010; Fussner *et al.*, 2011, 2012). The ChromEMT study was also consistent with the conclusions of a superresolution immunofluorescence study of mammalian stem cells (Ricci *et al.*, 2015). In summary, the structure of chromatin of mammalian cells is also irregular.

The alternative polymer-melt hypothesis predicts that the crowdedness of the nucleoplasm in vivo prevents chromatin fibers from individualizing into 30-nm fibers (Eltsov *et al.*, 2008). To test this hypothesis, we used cryo-ET to determine whether 30-nm-fiber formation is a conserved, intrinsic property of natural undigested chromatin liberated from picoplankton and yeast cells. In other words, can the chromatin of cells that do not show evidence of 30-nm fibers in vivo be made to adopt 30-nm-fiber structures in vitro? If chromatin in vitro forms large quantities of regular 30-nm fibers, then their absence in vivo could arise from the intracellular crowdedness that is cited by the polymer-melt hypothesis. If instead regular fibers are rare in vitro, then 30-nm fibers are not a stable conformation of natural chromatin

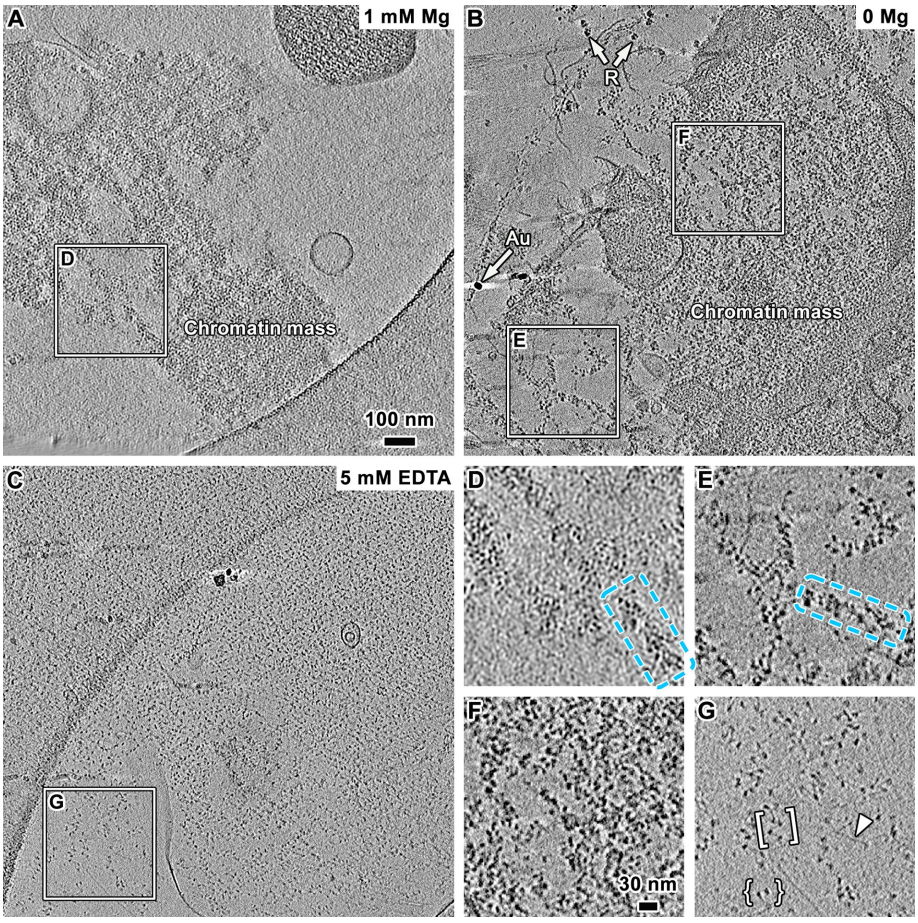

FIGURE 2: Picoplankton chromatin can form masses and irregular 30-nm fibers in the presence of divalent cations. Tomographic slices (30 nm) of picoplankton cell lysates in buffer supplemented with (A) 1 mM Mg, (B) no additional Mg, and (C) 5 mM EDTA. The dense puncta are gold fiducials (Au in B); the gently curved structures in A and C are the edges of the carbon support film. A couple of ribosomes (R) are indicated with arrows in B. Positions boxed in A–C are enlarged twofold, showing chromatin aggregates (D), short irregular 30-nm fibers (E, F), and open zigzags (G, bracket). A long stretch of naked DNA is indicated with an arrowhead in G. More examples of chromatin subjected to each condition are shown in Supplemental Figures S2–S4.

in vitro. We find that in the presence of even traces of divalent cations, most of the chromatin in both organisms condense into large masses. Some of the chromatin does form 30-nm fibers, predominantly of the irregular variety. In the absence of divalent cations, picoplankton chromatin decondenses into open zigzags, but to our surprise, yeast chromatin remains largely in a mass. To determine how these nucleosomes interact, we performed two-dimensional and three-dimensional classification and found that there is no dominant higher-order packing motif. Therefore, the structure of natural chromatin is irregular and sensitive to environmental conditions.

RESULTS

Release of natural picoplankton chromatin

To study the higher-order structure of natural picoplankton chromatin in vitro, we lysed cells in hypotonic buffer on ice, either with or without divalent cations (Figure 1B). This treatment released all cellular contents, including the chromatin, and is expected to produce thinner plunge-frozen samples that can lead to higher-contrast cryotomograms. Nuclei could not be isolated because the picoplankton nucleus is semiopen (Henderson *et al.*, 2007; Gan *et al.*, 2011). Compared to intact cells (Figure 1C), the lysed cells' contents spread over a much larger area and allowed the ice to be thinner, resulting in higher-contrast cryotomograms (Figure 1D). The majority of the densities are from remnants of the two largest organelles—the nucleus and the chloroplast. To keep the chromatin as intact as possible, we did not perform any isolation procedures or nuclease digestion.

Picoplankton chromatin forms masses and irregular 30-nm fibers only in the presence of divalent cations

Previous studies have shown that the structure of short nucleosome arrays is sensitive to divalent cations (Bednar *et al.*, 1998). To test whether undigested picoplankton chromatin can form 30-nm fibers, we imaged picoplankton lysates in the presence of varying concentrations of divalent cations (Figure 2, A–C). In 1 mM additional magnesium (Mg), most of the chromatin was condensed into a large thick mass, while a small portion of the chromatin formed irregular 30-nm fibers (Figure 2, A and D, and Supplemental Figure S1). Because the ice was so thick in these samples, the contrast was too low to reveal more details. We also lysed cells without additional Mg, leaving only trace amounts of divalent cations. Under this condition, most of the chromatin still remained part of a large compact mass, but short irregular 30-nm fibers were more abundant (Figure 2, B, E, and F, and Supplemental Figure S2). As a consequence of the ice thickness and dense nucleosome packing, the contrast was still too low to permit the unambiguous visualization of individual nucleosomes in most cryotomograms. We nevertheless found rare examples of nucleosome packed by regular face-to-face interactions into small clusters (Supplemental Figure S2, G–J).

To determine whether picoplankton chromatin masses and irregular 30-nm fibers require divalent cations, we chelated the residual divalent cations by lysing cells in the presence of 5 mM EDTA (Figure 2C and Supplemental Figure S3). The EDTA treatment was effective because ribosomes, which require Mg for stability (Chao, 1957), were no longer present (Figure 2, B and C). In picoplankton samples treated this way, we did not find any evidence of 30-nm fibers or chromatin masses. Instead, all of the chromatin was decondensed into open zigzags in which individual nucleosomes and naked linker DNA were visible (Figure 2G). Digested chicken-erythrocyte chromatin is a well-studied system that has divalent cation-dependent folding and can reproducibly form compact 30-nm fibers in the presence of Mg. To control for the effects of the buffer conditions used here and in experiments reported below, we also resuspended chicken-erythrocyte chromatin in a range of Mg- or EDTA-containing buffers. Cryo-ET of these control samples showed the expected 30-nm fibers in the presence of Mg and open zigzags in the presence of EDTA (Supplemental Figure S4). Therefore, like chicken-erythrocyte chromatin, picoplankton chromatin higher-order structure is very sensitive to divalent-cation concentration.

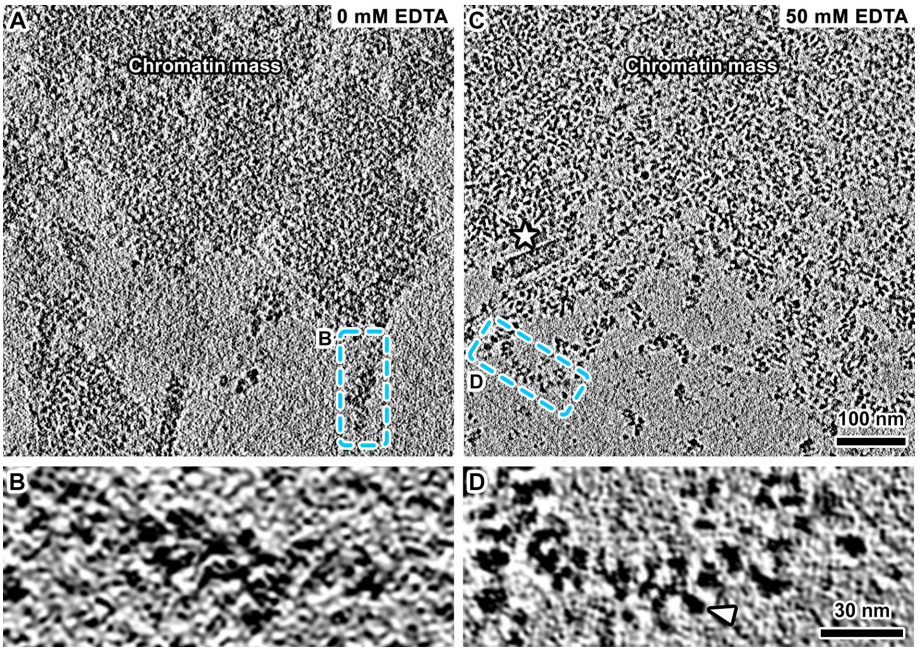

FIGURE 3: Yeast chromatin forms masses and irregular 30-nm fibers even in the absence of divalent cations. (A) Tomographic slices (30 nm) of yeast nuclei lysates without EDTA. (B) Enlargement (fourfold) of the irregular 30-nm fiber boxed in A. (C) Tomographic slices (30 nm) of yeast nuclei lysates in 50 mM EDTA. Star, microtubule. (D) Enlargement (fourfold) of the irregular 30-nm fiber boxed in C. Arrowhead, nucleosome.

Yeast chromatin packing is less sensitive to divalent cations than picoplankton

Picoplankton and yeast chromatin do not show evidence of 30-nm fibers in vivo (Gan *et al.*, 2013; Chen *et al.*, 2016). To test whether yeast chromatin structure is also sensitive to divalent cations in vitro, we attempted to image chromatin in yeast lysates. Yeast chromatin was more difficult to locate in this kind of sample, because there was no high-contrast chromatin-proximal structure like the chloroplast. To overcome this problem, we first isolated and then lysed the nuclei in hypotonic buffer without additional divalent cations (Supplemental Figure S5). This strategy made it straightforward to locate the chromatin, which became the most abundant material on the grid. Like picoplankton, yeast chromatin samples were thicker in the presence of additional Mg and had such low contrast that nucleosomes could not be resolved (Supplemental Figure S6A).

In the absence of additional Mg, the majority of yeast chromatin was also condensed in a thick mass (Figure 3A and Supplemental Figure S6B). Cryotomograms of this chromatin mass had low contrast, which prevented us from visualizing individual nucleosomes. In rare cases, we saw irregular 30-nm fibers at the periphery of the chromatin mass (Figure 3B). In total, we observed only seven irregular 30-nm fibers in 11 cryotomograms. Therefore, in the presence of trace amounts of free Mg, yeast chromatin is condensed in vitro and can occasionally form irregular 30-nm fibers.

To determine how yeast chromatin is organized in the absence of divalent cations, we lysed nuclei in the presence of EDTA. In the 5 mM EDTA-treated sample, we were unable to distinguish most nucleosomes because the chromatin was not dispersed enough (Supplemental Figures S6C and S7, A–C). Trace amounts of divalent cations were still present in this condition because ribosomes could still be found (Supplemental Figure S7B). We therefore increased the lysis buffer's EDTA concentration to 15 and 50 mM. We found ribosomes in 15 mM EDTA but not in 50 mM EDTA, meaning that the latter condition better sequestered the free divalent cations (Supplemental Figures S6, D and E, and S7D). In the presence of 50 mM EDTA, the chromatin mass was more dispersed (Figure 3C and Supplemental Figure S6E). Some chromatin at the periphery was compacted as irregular fibers but they were still rare (Figure 3D). The preparation of 50 mM EDTA at neutral pH requires the addition of a large quantity of sodium hydroxide, which increases the concentration of the monovalent cation sodium. To control for the potential effects of a high sodium concentration in 50 mM EDTA, we diluted chromatin 10-fold into 5 mM EDTA. In this condition, divalent-cation chelation should be as effective as in 50 mM EDTA but with a 10-fold-lower sodium concentration. Chromatin diluted this way was just as disperse as in 50 mM EDTA without dilution, meaning that the yeast chromatin dispersion was more sensitive to divalent cations; ribosomes were also not observed, as expected (Supplemental Figure S6, E and F). Unlike picoplankton chromatin in the absence of divalent cations, the nucleosomes of yeast chromatin remained closely packed and were not found to adopt the open zigzags with visible linker DNA (Supplemental Figures S6 and S7, E and F). In summary, natural yeast chromatin can condense into a large mass and form irregular 30-nm fibers even in the absence of divalent cations.

Linker histone does not contribute to yeast chromatin self-association

The absence of decondensed open-zigzag yeast chromatin in vitro was unexpected given how open picoplankton chromatin was under similar conditions. These observations may be explained by genome differences, one being that picoplankton does not have linker histones, but yeast does (Downs *et al.*, 2003). Linker histones could restrict the angles between entering and exiting linker DNA, thereby disfavoring more open conformations (Thoma and Koller, 1977; Bednar *et al.*, 1998). To test whether linker histones are required for yeast chromatin to self-associate in vitro, we imaged the chromatin released from *hho1*Δ cells, in which the linker-histone gene is deleted. As in wild-type chromatin, this linker-histone-free chromatin became more dispersed when the divalent-cation concentration decreased (Supplemental Figure S8). Importantly, most of the *hho1*Δ chromatin remained self-associated even in 50 mM EDTA (Supplemental Figure S8). Linker histone therefore cannot explain the self-association of yeast chromatin in vitro.

Histone acetylation facilitates yeast chromatin decondensation

Histone acetylation changes the nucleosome's net charge and therefore affects the ability of chromatin fragments to oligomerize (Tse *et al.*, 1998). Yeast chromatin is known to be susceptible to deacetylation when cells are disrupted (Waterborg, 2000). To test whether the histone-acetylation levels in yeast chromatin in vitro were too low to support decondensed structures like open zigzags,

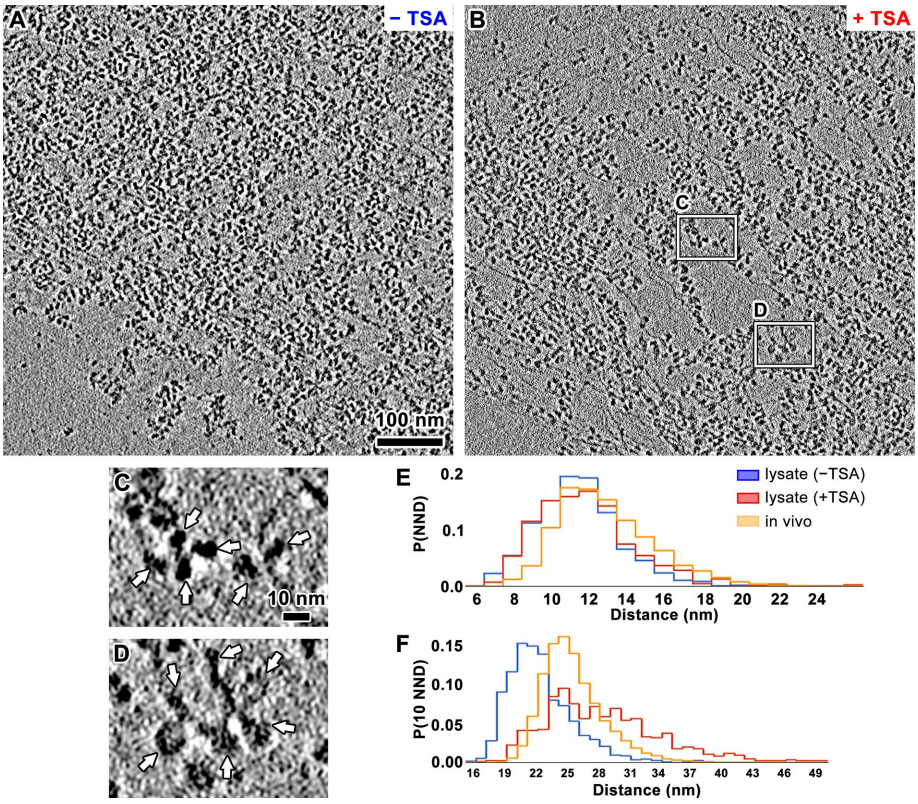

FIGURE 4: Yeast chromatin is more dispersed when histone deacetylases are inhibited. (A) Tomographic slice (10 nm) of a yeast nucleus lysed in buffer with 50 mM EDTA. (B) Tomographic slice (10 nm) of a yeast nucleus lysed in buffer with 50 mM EDTA and 82 μM TSA. (C, D) Fourfold enlargements of the positions boxed in white in B, showing decondensed chromatin fibers. Arrows, nucleosomes. (E, F) Histograms of nearest- and 10th-nearest-neighbor nucleosome distances, P(NND) and P(10 NND), respectively. The in vivo measurements were done using cryotomograms of cryosectioned yeast we previously reported (Chen *et al.*, 2016).

we treated the nuclei with trichostatin A (TSA), a histone-deacetylase inhibitor (Bernstein *et al.*, 2000). Cells treated this way had higher levels of H4 acetylation (Supplemental Figure S9A). We then lysed the nuclei in hypotonic buffer containing both EDTA and TSA. Chromatin isolated this way was indeed less condensed (Figure 4, A and B; more examples in Supplemental Figure S10, A and B) and, in rare cases, formed open zigzags (Figure 4, C and D). To further characterize the role of histone acetylation on nucleosome packing, we imaged the chromatin released from the histone-acetyltransferase double mutant *esa1*^{ts}*/gcn5*Δ, which has lower acetylation of histones H3 and H4 (Supplemental Figure S9B). The hypo-acetylated chromatin from these cells remained as a densely packed mass even in 50 mM EDTA (Supplemental Figure S11). Therefore, histone acetylation partially inhibits the self-association of natural chromatin.

To characterize nucleosome packing in a more objective way, we performed template matching of nucleosomes in vitro and of nucleosome-like densities in vivo (Chen *et al.*, 2016). We then analyzed the nearest-neighboring distance (NND) and the 10th NND (Figure 4, E and F; more examples of chromatin packing in vitro in Supplemental Figure S10, C and D). These two metrics are sensitive to nucleosome packing at different length scales (Supplemental Figure S12, A and B). The mean NND and 10th NND are, respectively, 1 and 5 nm longer in the in vitro chromatin of TSA-treated cells versus untreated cells ($p < 0.05$, $n = 4$, two-tailed t test). The mean 10th NND is 3 nm shorter in the chromatin in vitro (without TSA treatment) than in vivo ($p < 0.05$, $n = 4$, two-tailed t test), while their mean NNDs are indistinguishable ($p > 0.05$, $n = 4$, two-tailed t test). Note, however, that template matching in vivo produces more false positives due to lower contrast and the presence of more nonnucleosomal macromolecular complexes. These false positives cause NND (and 10th NND) values to be underestimated, meaning that chromatin is even less condensed in vivo than our analysis would suggest. To better understand these nucleosome-packing results, we simulated clusters of nucleosomes in which the three-dimensional positions were drawn from a uniform distribution and separated by at least 10 nm (Supplemental Figure S12, C, D, G, and H). We varied both the number of nucleosomes per cluster and the size of the gap between the clusters. We found that bigger gaps between clusters increased the 10th NND but not the NND (Supplemental Figure S12, E and F). Furthermore, the 10th NND is less sensitive to gap size if there are more nucleosomes per cluster (Supplemental Figure S12, I and J). Our NND analyses help explain the chromatin's appearance in vitro: histone acetylation barely changes short-range nucleosome packing but does increase the distance between groups of nucleosomes.

Natural chromatin has few ordered positions

The crystal structure of a tetranucleosome and the cryo-EM structures of 30-nm fibers both have zigzag motifs with face-to-face nucleosome packing (Schalch *et al.*, 2005; Song *et al.*, 2014). In yeast chromatin, we found that only a few nucleosomes were packed face-to-face (Figure 5A) or in a zigzag motif (Figure 5B). To test whether there were more regular packing motifs, we used RELION (regularized likelihood optimization) to perform reference-free two-dimensional classification on subtomograms that contained multiple nucleosomes (Figure 5C). This approach simultaneously aligns and classifies cryotomographic slices (each treated like a windowed single-particle cryo-EM projection image) to produce class averages that maximize the probability of observing the entire set of cryotomographic slices. In agreement with our visual inspection, only one class average showed face-to-face packing. Furthermore, there was no dominant motif, which is expected of irregularly packed chromatin (Figure 5C).

Artificial chromatin arrays with a yeastlike 167–base pair nucleosome-repeat length are organized as compact 30-nm fibers (Routh *et al.*, 2008). To test whether natural yeast chromatin fibers (Figure 5D) are as compact as these artificial 30-nm fibers, we determined the number of nucleosomes per 11 nm in the fibers where individual nucleosomes are resolved (Figure 5E). Compared to the artificial fibers, most natural fibers are less compact (~1.3–3.2 vs. 6.1 nucleosomes per 11 nm; Figure 5E) and have a broader distribution of diameters (15–45 nm vs. 15–25 nm; Figure 5E). The two best-resolved picoplankton 30-nm fibers (Supplemental Figure S2, G and H) were also loosely packed (3.3 and 2.4 nucleosomes/11 nm). Therefore, natural chromatin fibers are less compact and more conformationally heterogeneous than artificial fibers.

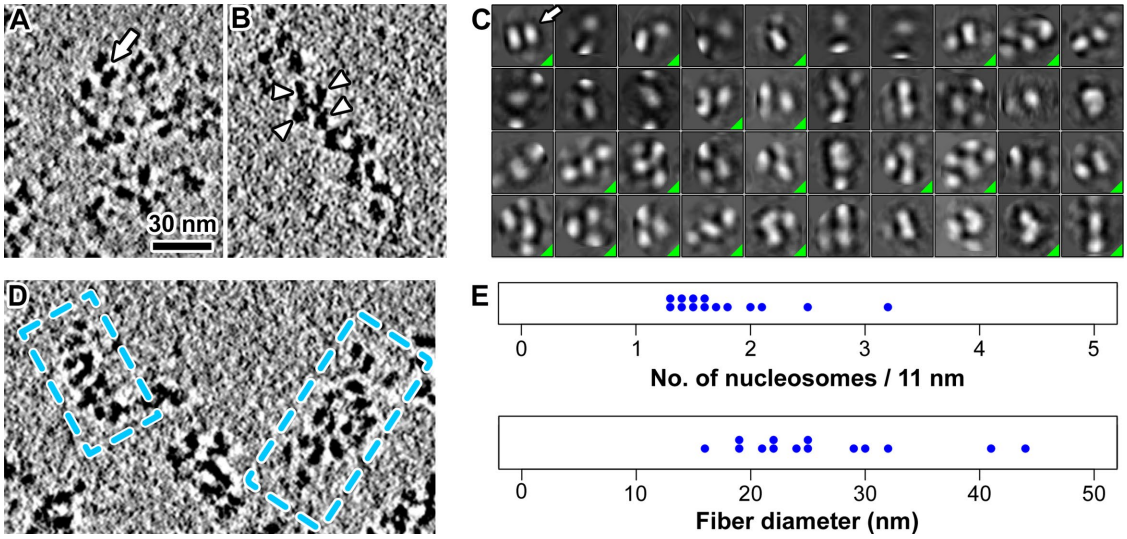

FIGURE 5: Yeast natural chromatin adopts few regular packing motifs. (A) Tomographic slice (10 nm) of yeast chromatin showing face-to-face packing (arrow). (B) Tomographic slice (6 nm) of yeast chromatin showing nucleosomes packed in a zigzag motif. Arrowheads, nucleosomes. (C) Two-dimensional class averages of yeast lysate in 50 mM EDTA, ordered left-to-right, top-to-bottom, from the most abundant to least abundant. Class averages that show nucleosome–nucleosome interactions have a lime-green triangle in the lower-right corner. Arrow, a class average showing face-to-face packing. (D) Tomographic slice (10 nm) of yeast irregular 30-nm fibers. (E) Distributions of fiber-condensation parameters.

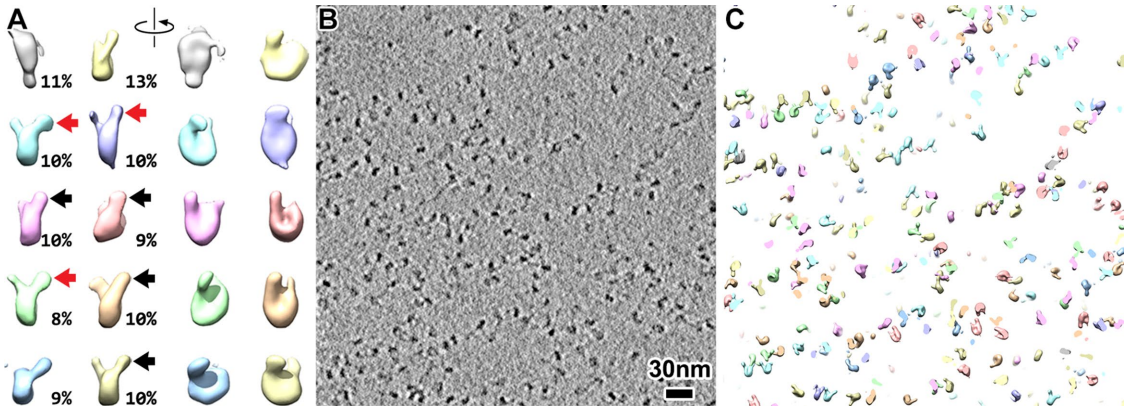

FIGURE 6: Picoplankton zigzag chromatin accommodates open linker DNA. (A) Gallery of nucleosome three-dimensional class averages viewed (left) edge on and (right) face on, contoured at 0.5σ to better visualize the linker DNA. The percentage of particles belonging to each respective class average is shown at the lower-right corner the corresponding density. Black arrows, classes with open linker DNA. Red arrows, class averages with crossed linker DNA. Notice that the upper yellow and lower blue class averages only show the density of one linker DNA. (B) Tomographic slice (20 nm) of *O. tauri* chromatin in lysis buffer with 5 mM EDTA. (C) Three-dimensional class averages of template-matched nucleosomes (same field as in B), remapped as a synthetic tomogram.

Natural chromatin has variable linker DNA conformations

The irregular packing of natural chromatin could be explained if the nucleosomes are themselves conformationally heterogeneous. To test this hypothesis, we developed a subtomogram analysis workflow that takes advantage of recent advances in three-dimensional image classification in RELION (Figures 6 and 7 and Supplemental Figures S13 and S14) (Bharat and Scheres, 2016). As implemented in RELION, three-dimensional classification compensates for the effects of the tomographic "missing-wedge" artifact. Like the two-dimensional classification implementation, image alignment (in three dimensions) and classification are done simultaneously. The picoplankton nucleosome class averages did not have enough resolution to reveal the two gyres of DNA in the core, but most of the classes did reveal short linker DNA densities (Figures 6A). In two types of classes, the linker DNA strands frequently entered and exited the nucleosome core in an "open" instead of "crossed" conformation (Figure 6A, black and red arrows, respectively; Supplemental Movie S1). In the third type of class, only one of the two linker DNAs was visible. In all class averages, the linker DNA is shorter than expected from the nucleosome repeat length (<7 nm), further supporting the conclusion that picoplankton linker-DNA conformation is variable. By contrast, linker DNA was not visible in any of the yeast nucleosome three-dimensional class averages, which were slightly higher resolution, with some averages featuring the DNA gyres (Figure 7A). These DNA gyres are absent in other yeast nucleosome three-dimensional class averages, which may result from proteins

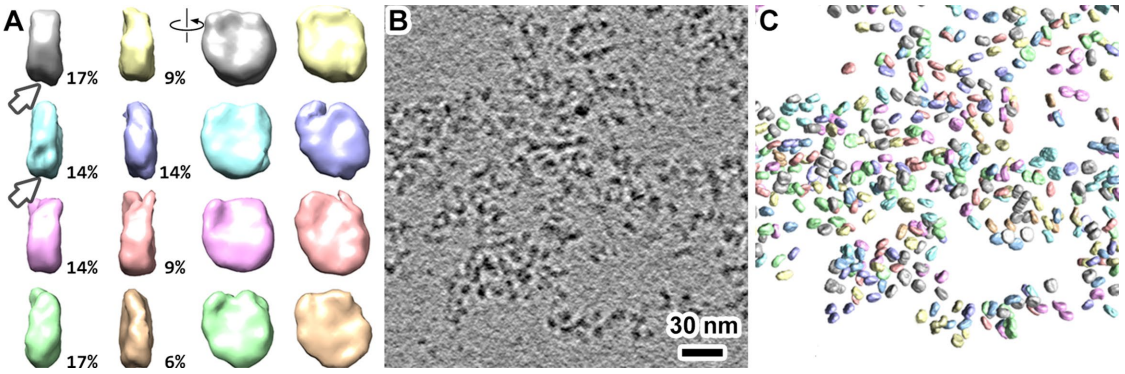

FIGURE 7: Yeast chromatin is heterogeneous at the mononucleosome and oligonucleosome levels. (A) Gallery of nucleosome three-dimensional class averages viewed (left) edge on and (right) face on. Arrows, groove between DNA gyres. Arrowhead, DNA stemlike structure. The color scheme has no relationship with Figure 6. (B) Tomographic slice (10 nm) of yeast nuclei lysates in the presence of 50 mM EDTA. (C) A synthetic tomogram (78 nm thick) of the tomogram position shown in B.

bound at that position or small distortions of those nucleosomes. Our three-dimensional classification of *hho1*Δ yeast nucleosomes did not reveal any notable differences relative to wild type (Supplemental Figure S15). In the nucleosomes of natural picoplankton and yeast chromatin, the linker DNA is therefore the most structurally variable feature.

Even though some of our cryotomograms reveal the locations of individual nucleosomes, they are still so crowded that we may have missed some higher-order motifs during visual inspection. To better visualize the higher-order packing of nucleosomes, we remapped the class averages of template-matched nucleosomes into a phantom volume the same size of the original cryotomogram to make a "synthetic tomogram." This approach is similar to the work done on polysomes and purified oligonucleosomes (Brandt *et al.*, 2009; Scheffer *et al.*, 2012). Most of the nucleosomes in divalent-cation-free buffer were visualized in the synthetic tomograms (Figures 6, B and C, and 7, B and C). In both picoplankton and yeast, the nucleosomes do not form long repeating motifs or regular structures of any kind (Figures 6C and 7C). Furthermore, there were no nucleosome clusters or chains formed by the same conformational class. This synthetic-tomogram analysis therefore supports the conclusion that natural chromatin conformation is irregular at the oligonucleosome level.

DISCUSSION

Our previous cryo-ET studies of picoplankton and yeast cells challenged the notion that the 30-nm fiber explained chromatin structure in vivo in unicellular eukaryotes. Compared to earlier cryo-EM work, which tested for periodic structures in two dimensions, cryo-ET can reveal the three-dimensional locations of individual nucleosomes. Furthermore, powerful maximum-likelihood-based classification algorithms can detect the presence or absence of regular motifs at both the single and oligonucleosome levels. Here, we have determined how natural chromatin is organized in vitro using undigested natural chromatin instead of the short chromatin fragments commonly used in other studies. This natural chromatin condenses as either irregular 30-nm fibers or masses at much lower divalent-cation concentrations than needed for chromatin fragments (Hansen, 2002; Maeshima *et al.*, 2016). In the absence of divalent cations, picoplankton chromatin decondenses to open zigzags, but yeast chromatin remains as masses and irregular 30-nm fibers. Notably, yeast chromatin did not unfold as much as expected. These observations suggest that the conformation of natural chromatin cannot be predicted from the behavior of chromatin fragments.

Picoplankton and yeast chromatin have different sensitivity to divalent cations

Sequestration of divalent cations with EDTA is known to disrupt 30-nm-fiber formation and oligomerization (Widom, 1986). We found that both picoplankton and yeast chromatin are more disperse in the absence of divalent cations. However, picoplankton chromatin adopts an open-zigzag conformation, whereas yeast chromatin is much more condensed with a few irregular 30-nm fibers in all conditions tested (Figure 8). The divalent cation-dependent picoplankton chromatin crowding is consistent with an earlier study of isolated HeLa chromosomes, which underwent "swelling" to an open zigzag form when Mg was sequestered (Eltsov *et al.*, 2008). By contrast, our natural yeast chromatin did not unfold as expected. In an early study (Lowary and Widom, 1989), yeast chromatin fragments in low salt formed uniformly thick "10-nm filaments," which can be explained if all sequential nucleosomes were stacked face to face (Figure 1A, structure vi). Because nucleosome stacking within the same chain requires the linker DNA to adopt highly curved, energetically unfavorable conformations, we believe the extended beads-on-a-string (Figure 1A, structure v) is a more reasonable model for those 10-nm filaments. We did not observe either of these structures, probably due to the sample differences, for example, purified short yeast

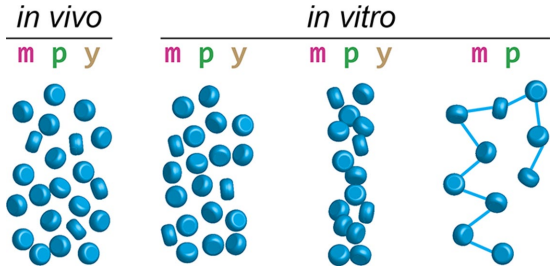

FIGURE 8: Chromatin packing is irregular in vitro. Chromatin packing in (m) metazoans, (p) picoplankton, and (y) yeast. In vivo, cryo-EM and cryo-ET data are most consistent with a chromatin mass. In isolated chromatin, masses (left), irregular 30-nm fibers (middle), and open zigzags (right) have been seen in all three classes of organisms except yeast.

chromatin fragments versus nuclear lysate, fixed versus unfixed chromatin, and adhesion to a substrate versus suspension in amorphous ice. In summary, natural picoplankton chromatin follows the divalent cation-dependent condensation behavior seen in metazoans, but yeast chromatin does not.

We have started to test the factors that could explain the differences between yeast and picoplankton chromatin structure in vitro. Using the *hho1Δ* strain, we ruled out linker histone, which is present in yeast but not picoplankton, as a factor that condenses chromatin in yeast. Another potential explanation could be the difference in the linker-DNA length. Both simulations and experiments with oligonucleosomes have shown that linker length has a profound impact on chromatin higher-order structure (Schalch *et al.*, 2005; Wong *et al.*, 2007; Collepardo-Guevara and Schlick, 2014; Ekundayo *et al.*, 2017). Because the yeast nucleosome-repeat length is ~30 base pairs shorter than picoplankton (Thomas and Furber, 1976; Gan *et al.*, 2013), sequential nucleosomes are closer together and therefore more likely to interact. Consistent with this idea, fission yeast chromatin, which has shorter linker DNA than budding yeast, also self-associates in vitro (Cai *et al.*, 2017). Finally, picoplankton linker DNA is enriched in methylation (Huff and Zilberman, 2014), which stiffens DNA (Nathan and Crothers, 2002). This stiffer linker DNA may also help to keep picoplankton nucleosomes apart as open zigzags in the absence of divalent cations.

Natural chromatin is irregular at multiple length scales

Linker DNA has variable length and variable nucleosome entry/exit angles (Yao *et al.*, 1990; Roulland *et al.*, 2016). In yeast, we could not detect the majority of the linker-DNA densities, probably due to the crowded packing of nucleosomes that lowers its contrast. In picoplankton chromatin, we detected linker DNA of differing orientations in three-dimensional nucleosome class averages. Unlike reconstituted nucleosome arrays (without linker histone) in which most nucleosomes had linker DNA in the "closed" conformation (Geiss *et al.*, 2014), picoplankton linker DNA adopts a more "open" conformation, possibly because this DNA is stiffer (see above). However, the class averages reveal linker DNA that is shorter than expected from the nucleosome repeat length, which can result from variability in linker DNA orientation and/or length. This structural variability can explain the absence of higher-order chromatin motifs in picoplankton.

Beads-on-a-string motifs are characterized by the large ~180° angle made by the linker DNA at the nucleosome's entry/exit points (Figure 1A, structure v). Repetition of this motif maximizes the distance between nucleosomes, resulting in maximum decondensation. This motif is common in chromatin dried onto carbon film (Olins and Olins, 1974; Grigoryev *et al.*, 2009) but rare in frozen-hydrated chromatin (Bednar *et al.*, 1998; Geiss *et al.*, 2014). We very rarely saw beads-on-a-string in our picoplankton chromatin and did not see a single example in our yeast chromatin. The most common decondensed conformation that natural chromatin can adopt in vitro is therefore the open zigzag.

Face-to-face nucleosome packing has been observed in oligonucleosome arrays (Robinson *et al.*, 2006) and isolated starfish sperm chromatin (Scheffer *et al.*, 2012). This form of packing is probably stabilized by the well-known interaction between a positively charged histone tail on one nucleosome with the acidic patch on a neighbor (Luger *et al.*, 1997a; Funke *et al.*, 2016). Here we found that the face-to-face interactions exist in both picoplankton and yeast but are rare. The rarity of face-to-face packing in natural chromatin is at odds with the cryo-EM models of recombinant 30-nm fibers, in which every single nucleosome is involved in a face-to-face packing interaction (Song *et al.*, 2014). In that study, the absence of histone marks, the glutaraldehyde fixation, and the regular spacing between sequential nucleosomes could have stabilized the face-to-face packing interaction, accounting for a key structural difference between reconstituted nucleosome arrays and natural chromatin.

An earlier study found that short nucleosome arrays with a yeast-like nucleosome-repeat length (167 base pairs) could form well-separated ordered 30-nm fibers in vitro (Routh *et al.*, 2008). We did not observe such fibers. Instead, most yeast nucleosomes pack into a large mass without any regular motifs; in rare cases, yeast chromatin packs as irregular 30-nm fibers. The formation of chromatin masses can be explained by the interdigitation of fibers, that is, nucleosomes from adjacent fibers interact, forcing the irregular 30-nm fibers to unfold (Eltsov *et al.*, 2008). In support of this idea, 30-nm fibers are found at the less-crowded periphery of chromatin masses in vitro. These masses could also be explained by hierarchical loops, which are compatible with heterogeneous packing (Grigoryev *et al.*, 2016). However, due to technical limitations, we cannot exclude the alternative possibility that the irregular 30-nm fibers do not unfold but are packed so closely that they are indistinguishable (Grigoryev and Woodcock, 2012).

The role of histone acetylation in yeast chromatin packing in vitro

Yeast chromatin was recalcitrant to decondensation in all of our sample-treatment conditions. Maximum nucleosome dispersal could only be achieved by the combination of TSA treatment and incubation with high EDTA concentration. Under these conditions, the hyperacetylated chromatin formed distinct fibers, suggesting that the interfiber contacts were weakened relative to hypoacetylated chromatin. The weakening of these contacts would allow nucleosome clusters to more easily glide by each other in the presence of external forces, potentially explaining the acetylation-dependent deformability of nuclei reported in a recent study (Shimamoto *et al.*, 2017).

Yeast chromatin is more condensed in vitro than in vivo

Our past and present cryo-ET studies give us a rare opportunity to compare three-dimensional chromatin organization in vitro and in vivo. One key difference is that yeast nucleosomes pack slightly closer in vitro than in vivo. What factors might explain this unexpected difference? One possibility is that positively charged cytoplasmic proteins bind to and facilitate chromatin condensation in the lysates. Alternatively, although our lysis approach is gentle, it cannot keep chromatin remodelers and transcription factors from dissociating from the chromatin. The presence of such factors in vivo might prevent the chromatin from folding into a more condensed structure. This notion was supported by a study showing that when the Widom 601 nucleosome-positioning element was inserted into the yeast genome, both the nucleosome positioning and the occupancy changed substantially compared with in vitro chromatin arrays (Perales *et al.*, 2011). We hypothesize that chromatin remodelers, transcription factors, and transcription itself keep chromatin dispersed in vivo; the absence of these factors in vitro allows chromatin to be more condensed.

MATERIALS AND METHODS

Picoplankton cell culture

Ostreococcus tauri cells (strain OTH95; Roscoff Culture Collection strain RCC 745) were grown in artificial seawater containing Sigma sea salt and Keller enrichment medium (Supplemental Table S1) in a 12 h:12 h light:dark cycle. Lighting was provided by T5050 white

light-emitting diodes, passed through a "Moonlight blue" filter (Lee Filters, #183; Panavision, Los Angeles, CA). This setup produced an illuminance of ~400–500 lux when measured at the approximate position of the cells with an Amprobe LM-100 digital light meter (Danaher, Everett, WA). Cells (30–50 ml) grown this way were loosely synchronized and were mostly in mid-G_1 phase at the beginning of the light phase (Corellou *et al.*, 2005). The cells were harvested in mid–log phase (OD_{600} ~ 0.05–0.1) shortly after the dark-to-light transition and then pelleted by centrifugation at 5000 × *g* for 10 min at 4°C.

Picoplankton lysis

Cells were then resuspended in 1 ml of prechilled (4°C) fresh artificial seawater and recentrifuged at 5000 × *g* for 1 min. The cell pellet was then resuspended in prechilled lysis buffer, yielding a final OD_{600} ~ 20. The cells were incubated on ice for either 7–9 min (1 mM Mg) or 10–15 min (0 Mg or 5 mM EDTA), measured from when the cells were resuspended in lysis buffer to the point of plunge freezing. Using a combination of sucrose and glycerol, the concentration of solutes (ions and undissociated molecules) in the lysis buffer was adjusted to ~820 mM, which is ~4/5 of the concentration of solutes in artificial seawater (~1 M); for details, see Supplemental Table S2. The picoplankton burst in all lysis buffers. While the plasma membrane was completely ruptured, the contents of the two largest organelles—the nucleus and the chloroplast—remained physically associated. This association was fortuitous, because the chloroplast remnants, which were high contrast and could be located even at low magnification, facilitated the search for the adjacent chromatin.

Yeast nucleus isolation and lysis

Nuclei were isolated using the Yeast nuclei isolation kit (Abcam 206997), with modifications. Wild-type yeast, strain YEF473A, was a gift from Kerry Bloom (University of North Carolina at Chapel Hill) (Bi and Pringle, 1996); the *esa1*ts/*gcn5*Δ histone-acetyltransferase double mutant, strain H4287, was a gift from Alan Hinnebusch (National Institute of Child Health and Human Development) (Ginsburg *et al.*, 2009); and the *hho1*Δ linker-histone deletion mutant was acquired from the American Type Culture Collection (ATCC 4002125). All cells were grown in 30 ml yeast peptone dextrose (YPD) medium to mid–log phase (OD_{600} ~ 1) in a shaker (30°C, 250 rpm). The cells were pelleted by centrifuging at 3000 × *g* for 5 min at room temperature in 50-ml conical tubes, washed twice by resuspension in 1 ml H_2O, and then recentrifuged at 3000 × *g* for 1 min. For *esa1*ts/*gcn5*Δ cells, the culture was transferred to 36°C for 4 h prior to harvesting. The cell pellet was then resuspended in 1 ml Buffer A (containing 10 mM dithiothreitol [DTT], from the kit) and then incubated for 10 min in a 30°C water bath. Cells were then centrifuged at 1500 × *g* for 5 min and then resuspended in 1 ml Buffer B (from the kit) containing lysis enzyme cocktail (diluted 1:1000). The mixture was incubated in a 30°C shaker for 15 min and then centrifuged at 1500 × *g* for 5 min at 4°C. The pellet was resuspended in 1 ml prechilled Buffer C (from the kit) with protease inhibitor cocktail. The suspension was transferred to a glass Dounce homogenizer on ice and then the cells were lysed with 15 strokes. The suspension was incubated with shaking for 30 min at room temperature and was then centrifuged at 500 × *g* for 5 min at 4°C to remove the debris. A small aliquot of the supernatant was stained with 4′,6-diamidino-2-phenylindole dihydrochloride to verify that the isolated nuclei were abundant. The supernatant was then recentrifuged at 20,000 × *g* for 10 min at 4°C. Finally, the nuclear pellet was resuspended in prechilled lysis buffer (Supplemental Table S2) and incubated for 15 min on ice prior to plunge freezing.

Chicken erythrocyte chromatin isolation

Chicken blood was acquired from a commercial source with approval of the Agri-Food and Veterinary Authority of Singapore. To prevent coagulation, heparin (Sigma, H3393) was added to fresh chicken blood to a final concentration of 50 U/ml. The isolation of chicken erythrocyte chromatin was performed as previously described, with modifications (Maeshima *et al.*, 2014). Briefly, 1 ml of fresh chicken blood was added to 10 ml of MLB (60 mM KCl, 15 mM NaCl, 15 mM 4-[2-hydroxyethyl]-1-piperazineethanesulfonic acid, pH 7.3, 2 mM $MgCl_2$, 0.1% NP-40, and 1 mM phenylmethylsulfonyl fluoride [PMSF]) and incubated for 10 min on ice. The lysate was washed three times by pelleting at 1000 × *g* at 4°C for 5 min and resuspending in 10 ml MLB. The pellet (nuclei) appeared light red after the washing steps. The nuclei were resuspended in 1 ml nuclei isolation buffer (10 mM Tris-HCl, pH 7.5, 1.5 mM $MgCl_2$, 1.0 mM $CaCl_2$, 0.25 M sucrose, 0.1 mM PMSF) and then digested with 50 U of micrococcal nuclease (Worthington, Lakewood, NJ) at 35°C for 2 min. The reaction was stopped by the addition of ethylene glycol-bis(β-aminoethyl ether)-*N*,*N*,*N*′,*N*′-tetraacetic acid to 2 mM final concentration. The nuclei were washed with 1 ml nuclei isolation buffer and then lysed on ice for 1 h with 1 ml lysis buffer (10 mM Tris-HCl, pH 7.5, 5 mM EDTA, 0.1 mM PMSF). The histones were verified to be intact by SDS–PAGE and the DNA fragmentation was checked with a 2% agarose gel. Ten microliters of the lysate was then dialyzed against dialysis buffer with different EDTA concentrations (10 mM Tris-HCl, pH 7.5, 0.1/5/50 mM EDTA, 0.1 mM PMSF) or with 1 mM Mg and 0.1 mM PMSF at 4°C overnight.

TSA treatment

Wild-type yeast were grown in 30 ml YPD to mid–log phase (OD_{600} ~ 1) in a shaker (30°C, 250 rpm). Cells were pelleted at 3000 × *g* for 5 min and then resuspended in 30 ml YPD with 16.4 μM TSA (5 mM stock in DMSO; Sigma T1952). The cells were then incubated for 1 h at 30°C before nuclei isolation. During nuclei isolation, the solutions used up to and including the spheroplasting step did not contain TSA. After spheroplasting, all solutions contained 82 μM TSA.

Western blot

Log-phase cells (~30 ml) were harvested by centrifuging at 5000 ×*g* for 5 min. The pellet was resuspended in 100 μl Laemmli sample buffer (Bio-Rad 1610737) and heated to 95°C for 10 min. The lysate was quick-spun and the supernatant was saved. Proteins were separated by SDS–PAGE in a 15% gel and transferred to polyvinylidene difluoride membrane. All blocking and antibody incubations were performed in Tris-buffered saline containing 0.5% Tween-20 and 2% (wt/vol) bovine serum albumin (BSA). The primary antibodies were rabbit anti-histone H3 (Abcam 1791), rabbit anti-acetyl-histone H3 (Millipore 06-599), and rabbit anti-acetyl-histone H4 (Millipore 06-866). The secondary antibodies were HRP-conjugated goat-anti-rabbit immunoglobulin G (CST 7074S). The blot membrane was treated with 1 ml Clarity Western ECL substrates (Bio-Rad 1705060) and scanned with a Thermo Scientific myECL Imager.

Plunge-freezing

Colloidal gold (used for fiducial-based cryo-ET image alignment; see below) tends to aggregate in the presence of seawater unless first treated with BSA (Gan *et al.*, 2011). Therefore, the gold (20 nm, BBI solutions, Cardiff, UK) was first suspended in 10 mg/ml BSA and then pelleted at 18,000 × *g* for 5 min. The supernatant was then discarded. The gold was treated with BSA twice in this way. The BSA-treated gold was then added to the cells just before plunge-freezing.

Grids (CF-4/2-2C-T and CF-2/2-2C-T; Protochips, Morrisville, NC) were plasma cleaned 45 or 90 s at 15 mA with a Emitech K100X glow-discharge unit. Cells or chromatin (3 µl) were added to one side (yeast) or both sides (6 µl total, picoplankton) of a plasma-cleaned grid. The grids were blotted with filter paper (Whatman, Grade 1) for 1 s, blot force 1, followed by a 5-s wait time, and then plunged into 67/33 (% vol/vol) liquid propane/ethane mixture (Tivol *et al.*, 2008) using a Vitrobot, Mark IV (Thermo, Waltham, MA). The relative humidity and the temperature in the sample chamber of the Vitrobot were kept at 100% and 4°C, respectively. The grids were then stored in liquid nitrogen.

Cryo-ET and image processing

Data-collection parameters and cryotomogram details are reported in Supplemental Tables S3 and S4, respectively. Tilt-series alignment and tomographic reconstruction were done using Etomo (Mastronarde, 1997). Because only the positions corresponding to the nuclear contents were of interest and because some sample positions warped during data collection, most tilt-series were aligned using only the gold fiducials in the vicinity of the nuclear densities. Some of the beads were automatically removed with the Etomo *bead eraser* tool. For yeast samples, all tilt series were aligned using patch tracking. For yeast and picoplankton samples treated with 0 mM Mg or with EDTA, the tilt series were first compensated for the effects of the contrast-transfer function and then two-dimensional low-pass filtered with cutoff in the range of 0.2–0.35 pixel^{-1} and sigma value of 0.05 pixel^{-1}; these settings attenuated the spatial-frequency components starting at 4.5-nm (picoplankton) to 2.6-nm (yeast) resolution. For picoplankton samples treated with 1 mM Mg, the contrast was much lower due to sample thickness and crowding effects, necessitating the twofold binning of the tilt series to improve the visualization. Other parameters were kept as Etomo defaults.

Template matching

Template matching was done using PEET (particle estimation for electron tomography) (Nicastro *et al.*, 2006; Heumann, 2016). Two types of templates were used: for picoplankton, a featureless cylinder (10-nm diameter, 6 nm thick) generated using the Bsoft program *beditimg* (Heymann and Belnap, 2007); for yeast, a subtomogram of a high-contrast nucleosome-like particle was selected. The choice of reference did not influence the subsequent analysis of most particles because a low cross-correlation (CC) cutoff was used (see below). For *O. tauri*, we found that the hits were off-center for nucleosomes oriented with their superhelical axis nearly perpendicular to the ice surface. These nucleosomes were better centered when we used a low-pass-filtered RELION three-dimensional class average as a reference. To minimize the effects of neighboring densities, subvolumes were isolated with a cylindrical mask with a soft edge. To minimize the number of false negatives, we kept the template-matching hits that were spaced as close together as 6 nm, corresponding to face-to-face packed nucleosomes. This minimum distance resulted in many "overlapped" candidate nucleosomes (hits), of which one was removed automatically at each position at the end of the search. To further minimize the number of false negatives, all hits with a CC (relative to the template) greater than 0.2 were saved and then visualized in the original cryotomogram; the CC values were displayed using the 3dmod *fine grain* function. The CC cutoff was then manually increased in 0.05 increments until most spurious hits (carbon support edge, ice contaminants, and aggregates) were eliminated. The final filtered hit list was then subjected to heterogeneity analysis using RELION (see below).

Nearest-neighbor distance analysis

For a fair comparison between different data sets, we used the average of CC coefficients of all template-matching hits as the initial cutoff. For example, if the average CC value in data set A was 0.4 and the one in data set B was 0.3, then we used 0.4 as the cutoff for A and 0.3 for B. We then made small adjustments to the CC cutoff to ensure the low occurrence of obvious false positives and false negatives. The coordinates of the nucleosome hits were then imported into Matlab. NND and 10th NND were calculated using the Matlab function *nearestneighbour.m* (https://github.com/anaphaze/ot-tools).

Three-dimensional models corresponding to possible nucleosome distributions were generated by sampling from a uniform three-dimensional distribution. To simulate the steric effects of nucleosome packing, only those points separated by at least 6 nm were kept. Distributions were made to test a range of concentrations (model points per volume) and clusters (two sets of model points separated by a gap). These model points were subjected to the same NND analyses as above.

Heterogeneity analysis and subtomogram averaging

Subtomograms were analyzed using the subtomogram-averaging and classification routines (Bharat *et al.*, 2015; Bharat and Scheres, 2016) as implemented in RELION 1.4 and 2.0 (Scheres, 2012a,b; Kimanius *et al.*, 2016). Because contrast transfer function (CTF) phase flipping was already done in IMOD, we did not CTF correct in RELION. We also disabled the dose-weightage scheme because the images in the second half of some tilt series were severely underweighted due to the large cumulative dose. The missing-wedge effects were compensated for by the RELION CTF model. Candidate nucleosome positions were imported into RELION. Owing to the crowdedness of yeast nucleosomes, we used a smaller box (24 nm) and a smaller mask (17-nm diameter) for classification to exclude most densities of adjacent nucleosomes. Each nucleosome was averaged along the tomographic Z axis to produce a pseudoprojection. These projections were then subjected to two-dimesional classification (50 or 100 classes). "Junk" particles such as ice, contaminants, or carbon-support features were manually removed. If the identity of the class ("junk" vs. real nucleosome) was ambiguous, then the corresponding particle positions were visualized in the context of the original tomogram, allowing for discrimination of junk and real particles. Our decisions to exclude/include ambiguous classes were guided by biologically meaningful features such as the size and shape of the density and the proximity to the other nucleosomes (most chromatin-associated nucleosomes are not found "floating" alone). The remaining good particles were subjected additional rounds of two-dimensional classification and elimination of junk classes until only reasonable nucleosome-like classes remained.

To discriminate between nucleosome conformational states, we performed three-dimensional classification. Because picoplankton nucleosomes were so dispersed, we used a spherical mask and no reference. For yeast chromatin, which was extremely crowded, we used a cylindrical mask with a soft edge and a featureless cylindrical reference. New junk classes were found and removed at the end of each round of classification. We found that the number of nucleosome classes decreased as we increased the resolution used for classification to the Nyquist limit. This resolution dependency is probably due to the lower signal-to-noise ratio of the higher-resolution data. Starting with 20 classes and using data to 20 Å resolution, fewer than 10 distinctive conformational classes remained at the end of two to three sequential classification-and-junk-removal rounds. These classes were then subjected to synthetic tomogram

construction. For picoplankton chromatin in 1 and 0 mM Mg, we also attempted three-dimensional classification of higher-order structures by increasing the mask size but found that most of the classes did not converge to anything biologically meaningful. Our two-dimensional classification of picoplankton chromatin in 5 mM EDTA failed to find any convincing face-to-face or other abundant higher-order motifs.

Synthetic tomogram construction

Template-matching hits that were subjected to classification analysis were mapped back into a phantom volume the same size of the original cryotomogram using the EMAN2 program *e2proc3d* (Tang *et al.*, 2007). These operations were done with the script *ot_remap.py* (https://github.com/anaphaze/ot-tools).

Statistical analysis

The *t* tests were performed in Google sheets and Microsoft Excel.

Figures

Density maps were rendered with UCSF Chimera (Pettersen *et al.*, 2004).

Data sharing

Tilt-series data of all samples presented in this paper are available at the EMPIAR online database (EMPIAR-10098). One example cryotomogram each of picoplankton and yeast has been deposited in the EMDB (EMD-6737).

ACKNOWLEDGMENTS

We thank the Centre for BioImaging Sciences microscopy staff for support and training, François-Yves Bouget for advice on *Ostreococcus* cell-culture conditions, Rado Danev for suggesting two-dimensional classification of subtomograms, Kerry Bloom and Alan Hinnebusch for yeast strains, Bee Ling Tay for help with chicken erythrocyte preparation, and the Gan team, Kazu Maeshima, and David Shore for discussions. S.C., Y.S., C.C., and L.G. were supported by National University of Singapore startups R-154-000-515-133, R-154-000-524-651, and D-E12-303-154-217, a MOE T2 R-154-000-624-112 and T1 R-154-000-A49-114, and a NUS YIA R-154-000-558-133.

REFERENCES

Athey BD, Smith MF, Rankert DA, Williams SP, Langmore JP (1990). The diameters of frozen-hydrated chromatin fibers increase with DNA linker length: evidence in support of variable diameter models for chromatin. J Cell Biol 111, 795–806.

Bednar J, Horowitz RA, Grigoryev SA, Carruthers LM, Hansen JC, Koster AJ, Woodcock CL (1998). Nucleosomes, linker DNA, and linker histone form a unique structural motif that directs the higher-order folding and compaction of chromatin. Proc Natl Acad Sci USA 95, 14173–14178.

Bernstein BE, Tong JK, Schreiber SL (2000). Genomewide studies of histone deacetylase function in yeast. Proc Natl Acad Sci USA 97, 13708–13713.

Bharat TA, Russo CJ, Lowe J, Passmore LA, Scheres SH (2015). Advances in single-particle electron cryomicroscopy structure determination applied to sub-tomogram averaging. Structure 23, 1743–1753.

Bharat TA, Scheres SH (2016). Resolving macromolecular structures from electron cryo-tomography data using subtomogram averaging in RELION. Nat Protoc 11, 2054–2065.

Bi E, Pringle JR (1996). ZDS1 and ZDS2, genes whose products may regulate Cdc42p in Saccharomyces cerevisiae. Mol Cell Biol 16, 5264–5275.

Brandt F, Etchells SA, Ortiz JO, Elcock AH, Hartl FU, Baumeister W (2009). The native 3D organization of bacterial polysomes. Cell 136, 261–271.

Cai S, Chen C, Tan ZY, Huang Y, Shi J, Gan L (2017). Cryo-ET reveals nucleosome reorganization in condensed mitotic chromosomes in vivo. bioRxiv. Retrieved January 1, 2018, from https://www.biorxiv.org/content/early/2017/11/24/178996.

Chao FC (1957). Dissociation of macromolecular ribonucleoprotein of yeast. Arch Biochem Biophys 70, 426–431.

Chen C, Lim HH, Shi J, Tamura S, Maeshima K, Surana U, Gan L (2016). Budding yeast chromatin is dispersed in a crowded nucleoplasm in vivo. Mol Biol Cell 27, 3357–3368.

Collepardo-Guevara R, Schlick T (2014). Chromatin fiber polymorphism triggered by variations of DNA linker lengths. Proc Natl Acad Sci USA 111, 8061–8066.

Collins N, Poot RA, Kukimoto I, Garcia-Jimenez C, Dellaire G, Varga-Weisz PD (2002). An ACF1-ISWI chromatin-remodeling complex is required for DNA replication through heterochromatin. Nat Genet 32, 627–632.

Corellou F, Camasses A, Ligat L, Peaucellier G, Bouget FY (2005). Atypical regulation of a green lineage-specific B-type cyclin-dependent kinase. Plant Physiol 138, 1627–1636.

Dorigo B, Schalch T, Bystricky K, Richmond TJ (2003). Chromatin fiber folding: requirement for the histone H4 N-terminal tail. J Mol Biol 327, 85–96.

Dorigo B, Schalch T, Kulangara A, Duda S, Schroeder RR, Richmond TJ (2004). Nucleosome arrays reveal the two-start organization of the chromatin fiber. Science 306, 1571–1573.

Downs JA, Kosmidou E, Morgan A, Jackson SP (2003). Suppression of homologous recombination by the Saccharomyces cerevisiae linker histone. Mol Cell 11, 1685–1692.

Ekundayo B, Richmond TJ, Schalch T (2017). Capturing structural heterogeneity in chromatin fibers. J Mol Biol 429, 3031–3042.

Eltsov M, Maclellan KM, Maeshima K, Frangakis AS, Dubochet J (2008). Analysis of cryo-electron microscopy images does not support the existence of 30-nm chromatin fibers in mitotic chromosomes in situ. Proc Natl Acad Sci USA 105, 19732–19737.

Eltsov M, Sosnovski S, Olins AL, Olins DE (2014). ELCS in ice: cryo-electron microscopy of nuclear envelope-limited chromatin sheets. Chromosoma 123, 303–312.

Finch JT, Klug A (1976). Solenoidal model for superstructure in chromatin. Proc Natl Acad Sci USA 73, 1897–1901.

Funke JJ, Ketterer P, Lieleg C, Korber P, Dietz H (2016). Exploring nucleosome unwrapping using DNA origami. Nano Lett 16, 7891–7898.

Fussner E, Djuric U, Strauss M, Hotta A, Perez-Iratxeta C, Lanner F, Dilworth FJ, Ellis J, Bazett-Jones DP (2011). Constitutive heterochromatin reorganization during somatic cell reprogramming. EMBO J 30, 1778–1789.

Fussner E, Strauss M, Djuric U, Li R, Ahmed K, Hart M, Ellis J, Bazett-Jones DP (2012). Open and closed domains in the mouse genome are configured as 10-nm chromatin fibres. EMBO Rep 13, 992–996.

Gan L, Ladinsky MS, Jensen GJ (2011). Organization of the smallest eukaryotic spindle. Curr Biol 21, 1578–1583.

Gan L, Ladinsky MS, Jensen GJ (2013). Chromatin in a marine picoeukaryote is a disordered assemblage of nucleosomes. Chromosoma 122, 377–386.

Geiss CP, Keramisanou D, Sekulic N, Scheffer MP, Black BE, Frangakis AS (2014). CENP-A arrays are more condensed than canonical arrays at low ionic strength. Biophys J 106, 875–882.

Ginsburg DS, Govind CK, Hinnebusch AG (2009). NuA4 lysine acetyltransferase Esa1 is targeted to coding regions and stimulates transcription elongation with Gcn5. Mol Cell Biol 29, 6473–6487.

Grigoryev SA, Arya G, Correll S, Woodcock CL, Schlick T (2009). Evidence for heteromorphic chromatin fibers from analysis of nucleosome interactions. Proc Natl Acad Sci USA 106, 13317–13322.

Grigoryev SA, Bascom G, Buckwalter JM, Schubert MB, Woodcock CL, Schlick T (2016). Hierarchical looping of zigzag nucleosome chains in metaphase chromosomes. Proc Natl Acad Sci USA 113, 1238–1243.

Grigoryev SA, Woodcock CL (2012). Chromatin organization—the 30 nm fiber. Exp Cell Res 318, 1448–1455.

Hansen JC (2002). Conformational dynamics of the chromatin fiber in solution: determinants, mechanisms, and functions. Annu Rev Biophys Biomol Struct 31, 361–392.

Hansen JC (2012). Human mitotic chromosome structure: what happened to the 30-nm fibre? EMBO J 31, 1621–1623.

Henderson GP, Gan L, Jensen GJ (2007). 3-D ultrastructure of O. tauri: electron cryotomography of an entire eukaryotic cell. PLoS One 2, e749.

Heumann JM (2016). PEET: University of Colorado Boulder. Retrieved January 1, 2018, from bio3d.colorado.edu/PEET/.

Heymann JB, Belnap DM (2007). Bsoft: image processing and molecular modeling for electron microscopy. J Struct Biol 157, 3–18.

Huff JT, Zilberman D (2014). Dnmt1-independent CG methylation contributes to nucleosome positioning in diverse eukaryotes. Cell 156, 1286–1297.

Huynh VA, Robinson PJ, Rhodes D (2005). A method for the in vitro reconstitution of a defined "30 nm" chromatin fibre containing stoichiometric amounts of the linker histone. J Mol Biol 345, 957–968.
Jenuwein T, Allis CD (2001). Translating the histone code. Science 293, 1074–1080.
Kimanius D, Forsberg BO, Scheres SH, Lindahl E (2016). Accelerated cryo-EM structure determination with parallelisation using GPUs in RELION-2. Elife 5.
Lowary PT, Widom J (1989). Higher-order structure of Saccharomyces cerevisiae chromatin. Proc Natl Acad Sci USA 86, 8266–8270.
Luger K, Mäder AW, Richmond RK, Sargent DF, Richmond TJ (1997a). Crystal structure of the nucleosome core particle at 2.8 Å resolution. Nature 389, 251–260.
Luger K, Rechsteiner TJ, Flaus AJ, Waye MM, Richmond TJ (1997b). Characterization of nucleosome core particles containing histone proteins made in bacteria. J Mol Biol 272, 301–311.
Maeshima K, Hihara S, Eltsov M (2010). Chromatin structure: does the 30-nm fibre exist in vivo? Curr Opin Cell Biol 22, 291–297.
Maeshima K, Imai R, Hikima T, Joti Y (2014). Chromatin structure revealed by X-ray scattering analysis and computational modeling. Methods 70, 154–161.
Maeshima K, Rogge R, Tamura S, Joti Y, Hikima T, Szerlong H, Krause C, Herman J, Seidel E, DeLuca J, *et al*. (2016). Nucleosomal arrays self-assemble into supramolecular globular structures lacking 30-nm fibers. EMBO J 35, 1115–1132.
Mastronarde DN (1997). Dual-axis tomography: an approach with alignment methods that preserve resolution. J Struct Biol 120, 343–352.
McBryant SJ, Adams VH, Hansen JC (2006). Chromatin architectural proteins. Chromosome Res 14, 39–51.
McDowall AW, Smith JM, Dubochet J (1986). Cryo-electron microscopy of vitrified chromosomes in situ. EMBO J 5, 1395–1402.
Nathan D, Crothers DM (2002). Bending and flexibility of methylated and unmethylated EcoRI DNA. J Mol Biol 316, 7–17.
Nicastro D, Schwartz C, Pierson J, Gaudette R, Porter ME, McIntosh JR (2006). The molecular architecture of axonemes revealed by cryoelectron tomography. Science 313, 944–948.
Nishino Y, Eltsov M, Joti Y, Ito K, Takata H, Takahashi Y, Hihara S, Frangakis AS, Imamoto N, Ishikawa T, Maeshima K (2012). Human mitotic chromosomes consist predominantly of irregularly folded nucleosome fibres without a 30-nm chromatin structure. EMBO J 31, 1644–1653.
Olins AL, Olins DE (1974). Spheroid chromatin units (v bodies). Science 183, 330–332.
Ou HD, Phan S, Deerinck TJ, Thor A, Ellisman MH, O'Shea CC (2017). ChromEMT: Visualizing 3D chromatin structure and compaction in interphase and mitotic cells. Science 357, eaag0025.
Perales R, Zhang L, Bentley D (2011). Histone occupancy in vivo at the 601 nucleosome binding element is determined by transcriptional history. Mol Cell Biol 31, 3485–3496.
Pettersen EF, Goddard TD, Huang CC, Couch GS, Greenblatt DM, Meng EC, Ferrin TE (2004). UCSF Chimera—a visualization system for exploratory research and analysis. J Comput Chem 25, 1605–1612.
Ricci MA, Manzo C, Garcia-Parajo MF, Lakadamyali M, Cosma MP (2015). Chromatin fibers are formed by heterogeneous groups of nucleosomes in vivo. Cell 160, 1145–1158.
Robinson PJ, Fairall L, Huynh VA, Rhodes D (2006). EM measurements define the dimensions of the "30-nm" chromatin fiber: evidence for a compact, interdigitated structure. Proc Natl Acad Sci USA 103, 6506–6511.
Roulland Y, Ouararhni K, Naidenov M, Ramos L, Shuaib M, Syed SH, Lone IN, Boopathi R, Fontaine E, Papai G, *et al*. (2016). The flexible ends of CENP-A nucleosome are required for mitotic fidelity. Mol Cell 63, 674–685.
Routh A, Sandin S, Rhodes D (2008). Nucleosome repeat length and linker histone stoichiometry determine chromatin fiber structure. Proc Natl Acad Sci USA 105, 8872–8877.
Schalch T, Duda S, Sargent DF, Richmond TJ (2005). X-ray structure of a tetranucleosome and its implications for the chromatin fibre. Nature 436, 138–141.
Scheffer MP, Eltsov M, Bednar J, Frangakis AS (2012). Nucleosomes stacked with aligned dyad axes are found in native compact chromatin in vitro. J Struct Biol 178, 207–214.
Scheffer MP, Eltsov M, Frangakis AS (2011). Evidence for short-range helical order in the 30-nm chromatin fibers of erythrocyte nuclei. Proc Natl Acad Sci USA 108, 16992–16997.
Scheres SH (2012a). A Bayesian view on cryo-EM structure determination. J Mol Biol 415, 406–418.
Scheres SH (2012b). RELION: implementation of a Bayesian approach to cryo-EM structure determination. J Struct Biol 180, 519–530.
Shimamoto Y, Tamura S, Masumoto H, Maeshima K (2017). Nucleosome-nucleosome interactions via histone tails and linker DNA regulate nuclear rigidity. Mol Biol Cell 28, 1580–1589.
Song F, Chen P, Sun D, Wang M, Dong L, Liang D, Xu R-M, Zhu P, Li G (2014). Cryo-EM study of the chromatin fiber reveals a double helix twisted by tetranucleosomal units. Science 344, 376–380.
Tang G, Peng L, Baldwin PR, Mann DS, Jiang W, Rees I, Ludtke SJ (2007). EMAN2: an extensible image processing suite for electron microscopy. J Struct Biol 157, 38–46.
Thoma F, Koller T (1977). Influence of histone H1 on chromatin structure. Cell 12, 101–107.
Thomas JO, Furber V (1976). Yeast chromatin structure. FEBS Lett 66, 274–280.
Tivol WF, Briegel A, Jensen GJ (2008). An improved cryogen for plunge freezing. Microsc Microanal 14, 375–379.
Tse C, Sera T, Wolffe AP, Hansen JC (1998). Disruption of higher-order folding by core histone acetylation dramatically enhances transcription of nucleosomal arrays by RNA polymerase III. Mol Cell Biol 18, 4629–4638.
van Holde K, Zlatanova J (1995). Chromatin higher order structure: chasing a mirage? J Biol Chem 270, 8373–8376.
Waterborg JH (2000). Steady-state levels of histone acetylation in Saccharomyces cerevisiae. J Biol Chem 275, 13007–13011.
Widom J (1986). Physicochemical studies of the folding of the 100 A nucleosome filament into the 300 A filament. Cation dependence. J Mol Biol 190, 411–424.
Wong H, Victor JM, Mozziconacci J (2007). An all-atom model of the chromatin fiber containing linker histones reveals a versatile structure tuned by the nucleosomal repeat length. PLoS One 2, e877.
Woodcock CL (1994). Chromatin fibers observed in situ in frozen hydrated sections. Native fiber diameter is not correlated with nucleosome repeat length. J Cell Biol 125, 11–19.
Woodcock CL, Frado LL, Rattner JB (1984). The higher-order structure of chromatin: evidence for a helical ribbon arrangement. J Cell Biol 99, 42–52.
Yao J, Lowary PT, Widom J (1990). Direct detection of linker DNA bending in defined-length oligomers of chromatin. Proc Natl Acad Sci USA 87, 7603–7607.